JCTC Journal of Chemical Theory and Computation

pubs.acs.org/JCTC Article

Simulating Open Quantum System Dynamics on NISQ Computers with Generalized Quantum Master Equations

Yuchen Wang, Ellen Mulvihill, Zixuan Hu, Ningyi Lyu, Saurabh Shivpuje, Yudan Liu, Micheline B. Soley, Eitan Geva,* Victor S. Batista,* and Sabre Kais*

Cite This: J. Chem. Theory Comput. 2023, 19, 4851−4862 Read Online

ACCESS | Metrics & More | Article Recommendations | Supporting Information

ABSTRACT: We present a quantum algorithm based on the generalized quantum master equation (GQME) approach to simulate open quantum system dynamics on noisy intermediate-scale quantum (NISQ) computers. This approach overcomes the limitations of the Lindblad equation, which assumes weak system−bath coupling and Markovity, by providing a rigorous derivation of the equations of motion for any subset of elements of the reduced density matrix. The memory kernel resulting from the effect of the remaining degrees of freedom is used as input to calculate the corresponding non-unitary propagator. We demonstrate how the Sz.-Nagy dilation theorem can be employed to transform the non-unitary propagator into a unitary one in a higher-dimensional Hilbert space, which can then be implemented on quantum circuits of NISQ computers. We validate our quantum algorithm as applied to the spin-boson benchmark model by analyzing the impact of the quantum circuit depth on the accuracy of the results when the subset is limited to the diagonal elements of the reduced density matrix. Our findings demonstrate that our approach yields reliable results on NISQ IBM computers.

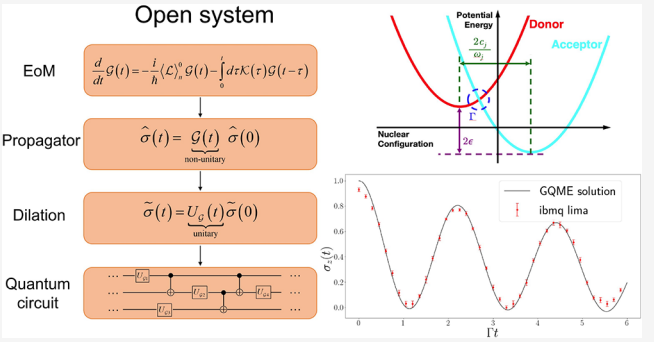

1. INTRODUCTION

Simulations of open quantum systems have become essential for studying the dynamics of quantum systems in the condensed phase, allowing for the inclusion of dissipative effects from the environment which are critical for accurate simulations. These powerful computational tools have enabled a wide range of studies, from chemical and physical processes to excited-state lifetimes, spectral diffusion, and line broadening, across multiple fields of research, including physical chemistry, molecular physics, condensed-phase physics, nanoscience, molecular electronics, quantum optics, nonequilibrium statistical mechanics, spectroscopy and quantum information science.[1−30] Examples of open quantum system dynamics include energy and charge transfer, dephasing, vibrational relaxation, nonadiabatic dynamics, and photochemistry (see Figure 1). By harnessing the power of open quantum system simulations, we can bridge the gap between theory and experiment, providing insight into various complex phenomena in a variety of light-induced physical and chemical processes, including photo-induced processes such as energy and charge transfer, vibronic relaxation, dephasing, and nonadiabatic dynamics.[22,23,28,31−49]

Recent advances in quantum computing have enabled the development of numerous algorithms for electronic structure calculations[50−53] and simulations of quantum dynamics of closed quantum systems.[54−57] However, relatively few studies have explored the simulation of open quantum system dynamics.[58−67] These studies have been mostly based on Lindblad-type quantum master equations (QMEs), which ensure complete positivity and conservation of probability but rely on the Markov and Born approximations in the system−bath weak coupling limit.[9] With the aim of developing a more general approach, here we introduce a quantum algorithm based on the generalized quantum master equation (GQME), which corresponds to the formally exact equation of motion (EoM) for an open quantum system.

A major challenge facing the quantum simulation of open quantum system dynamics is the fact that the time evolution operators are non-unitary whereas quantum gates are unitary. To this end, we have previously developed a quantum algorithm for open quantum dynamics based on the Sz.-Nagy unitary dilation theorem, which converts non-unitary operators into unitary operators in an extended Hilbert space. This algorithm was originally applied to simulating a Markovian two-level model on IBM quantum computers.[68] Later, the same method was applied to simulating the non-Markovian Jaynes−

Received: March 19, 2023
Published: May 26, 2023

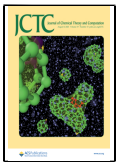

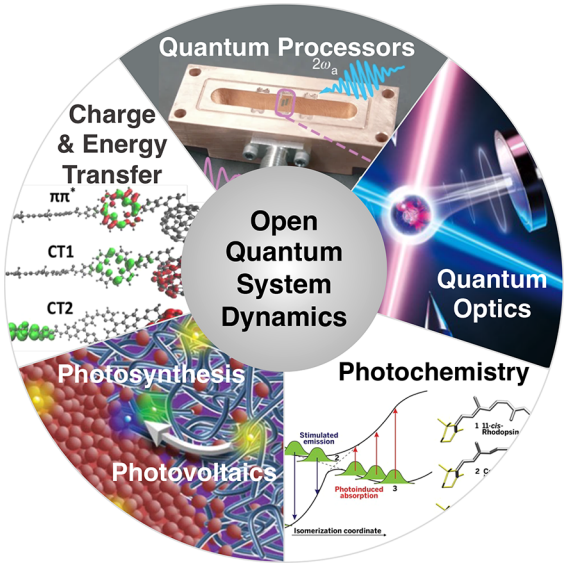

Figure 1. Simulation of open quantum system dynamics is central to many science and engineering disciplines (a few examples are showcased in the figure).

Cummings model on IBM quantum computers.[69] In a recent work, the same Lindblad-QME-based quantum algorithm was applied to simulate the dynamics of the Fenna−Matthews−Olson complex, which includes five quantum states and seven elementary physical processes.[70] Thus far, this quantum algorithm has been used to simulate the dynamics of open quantum systems described by the operator sum representation or Lindblad-type QMEs.

However, these approaches are not entirely general: the Lindblad QME used in ref 70 relies on several restrictive approximations, including Markovian dynamics, and the ensemble of Lindbladian trajectories method in ref 69, while capable of describing non-Markovian dynamics, involves user selection of *ad hoc* system−bath parameters, therefore limiting the range of applications. Furthermore, while the operator sum representation of open quantum system dynamics is general, it requires knowledge of the Kraus operators, which to the best of our knowledge are only known in closed form for systems whose dynamics can be described by Lindblad-type QMEs.

Extending the range of quantum simulation of open quantum systems therefore calls for formulating the dynamics within a less restrictive theoretical framework. The GQME formalism introduced by Nakajima[71] and Zwanzig[72] represents such a general framework since the GQME corresponds to the formally exact EoM of the open quantum system, as opposed to the Lindblad-type QMEs, which correspond to approximate EoMs of the open quantum system.

A comparison of the workflows for simulating the dynamics of a closed quantum system governed by the quantum Liouville equation *versus* an open quantum system governed by the GQME is shown in Figure 2. The derivation of the GQME involves projecting out the bath degrees of freedom (DOF) to obtain the EoM of the system's reduced density matrix, or a subset of its elements. Within this EoM, which is referred to as the GQME, the memory kernel superoperator, $\mathcal{K}(\tau)$, accounts for the main impact of the bath on the system's dynamics. Thus, the GQME replaces the Liouville equation as the formally exact EoM of the system when we transition from a closed quantum system to an open quantum system, with the memory kernel playing a similar role in the open system as the Hamiltonian or Liouvillian in the closed system.

In this work, we develop a GQME-based quantum algorithm for simulating the dynamics of an open quantum system. To this end, we develop a protocol for obtaining the non-unitary time evolution superoperator, or propagator, from the memory kernel. Then the Sz.-Nagy unitary dilation theorem is used to convert the GQME-based non-unitary propagator into a unitary superoperator in an extended Hilbert space. Given this dilated and now unitary time evolution superoperator and the initial state of the system, we can evolve the dynamics for any open quantum system on quantum computers.

Given the fact that the GQME is the exact EoM of the open quantum system, this quantum algorithm greatly extends the range of possible systems that can be simulated on a quantum computer, including complex non-Markovian photosynthetic and photovoltaic systems,[28,73] molecular electronics,[48] linear and nonlinear spectroscopy,[74] systems with intersystem crossing,[75] and conical intersections.[76] Thus, this GQME-based quantum algorithm provides an essentially universal protocol for

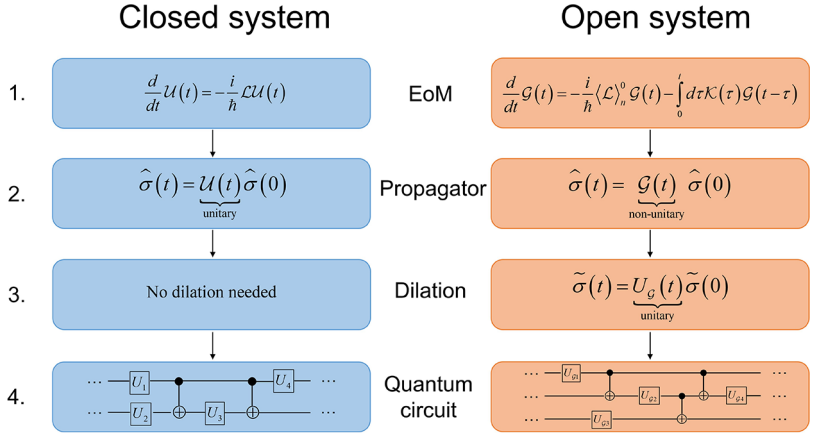

Figure 2. A comparison of the workflows for simulating the dynamics of a closed quantum system governed by the quantum Liouville equation *vs* an open quantum system governed by the GQME. 1. The EoM is established. 2. The time evolution superoperator is generated from the EoM. 3. A unitary dilation is required in order to convert the GQME-based non-unitary time evolution superoperator into a unitary superoperator in an extended Hilbert space. 4. The unitary matrix is translated into a quantum gate sequence.

https://doi.org/10.1021/acs.jctc.3c00316
J. Chem. Theory Comput. 2023, 19, 4851−4862

simulating open quantum system dynamics on quantum computing platforms. Given a powerful enough quantum computer, this algorithm opens the door for simulating open quantum system dynamics of large and complex molecular systems, which are currently beyond the reach of classical computers.

2. METHODS

2.1. GQME-Based Propagators. In this section, we outline our approach for calculating the GQME-based non-unitary propagator for the reduced density matrix of the open quantum system (see eq 9). The analogous procedure for calculating the non-unitary propagator for a subset of the reduced density matrix elements is outlined in section 3.2.

Previously developed quantum algorithms for open system dynamics involved mapping Lindblad operators to Kraus operators before using the Sz.-Nagy dilation theorem to reach a unitary quantum algorithm.[68−70] While useful for many systems, these methods are either Markovian[68,70] or involve user selection of *ad hoc* system−bath parameters,[69] therefore limiting the range of applications. In this paper, we introduce a method based on the GQME, a formally exact EoM for the dynamics of an open quantum system. Instead of casting the non-unitary propagator in terms of Kraus operators and dilating them, this method uses the GQME to obtain the system's time evolution superoperator, or propagator, $\mathcal{G}(t)$, and performs the dilation on it to obtain a unitary quantum algorithm. This subsection describes the first step in the workflow outlined in Figure 2, namely, obtaining the time evolution superoperator of an open quantum system starting from its formally exact EoM in GQME form.

For the sake of concreteness, we will focus on molecular systems with an overall Hamiltonian of the following commonly encountered form:

$$\hat{H} = \sum_{j=1}^{N_e} \hat{H}_j |j\rangle\langle j| + \sum_{\substack{j,k=1 \\ k\neq j}}^{N_e} \hat{V}_{jk} |j\rangle\langle k| \tag{1}$$

and an overall system initial state of the following commonly assumed single-product form:

$$\hat{\rho}(0) = \hat{\rho}_n(0) \otimes \hat{\sigma}(0) \tag{2}$$

With this assumption, the evolution is guaranteed to be described by a completely positive (CP) map.[60,77] It should be noted that the GQME approach is not limited to this form of Hamiltonian and initial state and that the choice to focus on them is solely motivated by clarity of presentation and the wide range of applications based on a Hamiltonian and initial state of this form. The system and bath in this case correspond to the electronic and nuclear DOF, respectively. In eqs 1 and 2, $\hat{H}_j = \hat{\mathbf{P}}^2/2 + V_j(\hat{\mathbf{R}})$ is the nuclear Hamiltonian when the system is in the diabatic electronic state $|j\rangle$, with the index j running over the N_e electronic states; $\hat{\mathbf{R}} = (\hat{R}_1, ..., \hat{R}_{N_n})$ and $\hat{\mathbf{P}} = (\hat{P}_1, ..., \hat{P}_{N_n})$ are the mass-weighted position and momentum operators of the $N_n \gg 1$ nuclear DOF, respectively; $\{\hat{V}_{jk} | j \neq k\}$ are the coupling terms between electronic states (which can be either nuclear operators or constants); and $\hat{\rho}_n(0)$ and $\hat{\sigma}(0)$ are the reduced density operators that describe the initial states of the nuclear (bath) and electronic (system) DOF, respectively. Throughout this paper, boldfaced variables (*e.g.*, $\mathbf{A}$) indicate vector quantities; a hat over a variable (*e.g.*, $\hat{B}$) indicates an operator quantity; and calligraphic font (*e.g.*, $\mathcal{L}$) indicates a superoperator.

Using projection operator techniques, one can then derive the following formally exact EoM, or GQME, for the reduced electronic density operator, $\hat{\sigma}(t)$:[27−30]

$$\frac{\mathrm{d}}{\mathrm{d}t}\hat{\sigma}(t) = -\frac{\mathrm{i}}{\hbar}\langle\mathcal{L}\rangle_n^0\hat{\sigma}(t) - \int_0^t \mathrm{d}\tau\, \mathcal{K}(\tau)\hat{\sigma}(t-\tau) \tag{3}$$

The open quantum system dynamics of the reduced electronic density matrix described by this GQME is generated by the two terms on the R.H.S. of eq 3. The first term is given in terms of the projected overall system Liouvillian $\langle\mathcal{L}\rangle_n^0 \equiv \mathrm{Tr}_n\{\hat{\rho}_n(0)\mathcal{L}\}$ (where $\mathcal{L}(\cdot) = [\hat{H}, \cdot]$ is the overall system Liouvillian and $\mathrm{Tr}_n\{\cdot\}$ is the partial trace over the nuclear (bath) Hilbert space), which is represented by an $N_e^2 \times N_e^2$ time-independent matrix. The second term is given in terms of the memory kernel $\mathcal{K}(\tau)$, which is represented by an $N_e^2 \times N_e^2$ time-dependent matrix.

The GQME formalism provides a general framework for deriving the exact EoM for any quantity of interest. The derivation begins with the Nakajima−Zwanzig equation,[71,72] which describes the dynamics of a projected state $\mathcal{P}\hat{\rho}(t)$, where $\mathcal{P}$ is a projection superoperator and $\hat{\rho}(t)$ is the density operator of the overall system:

$$\begin{aligned}\frac{\mathrm{d}}{\mathrm{d}t}\mathcal{P}\hat{\rho}(t) = &-\frac{\mathrm{i}}{\hbar}\mathcal{P}\mathcal{L}\mathcal{P}\hat{\rho}(t) \\ &- \frac{1}{\hbar^2}\int_0^t \mathrm{d}\tau\, \mathcal{P}\mathcal{L}\mathrm{e}^{-\mathrm{i}\mathcal{Q}\mathcal{L}\tau/\hbar}\mathcal{Q}\mathcal{L}\mathcal{P}\hat{\rho}(t-\tau) \\ &- \frac{\mathrm{i}}{\hbar}\mathcal{P}\mathcal{L}\mathrm{e}^{-\mathrm{i}\mathcal{Q}\mathcal{L}t/\hbar}\mathcal{Q}\hat{\rho}(0)\end{aligned} \tag{4}$$

Here $\mathcal{L}$ is the overall system−bath Liouvillian and $\mathcal{Q} = 1 - \mathcal{P}$ is the complementary projection superoperator to $\mathcal{P}$. Importantly, the only requirements are that $\mathcal{L}$ is Hermitian and $\mathcal{P}$ satisfies $\mathcal{P}^2 = \mathcal{P}$. Otherwise, there is complete flexibility in the choice of $\mathcal{L}$ and $\mathcal{P}$, with each choice leading to a different GQME for a different quantity of interest.[30]

Following ref 27, we focus an overall system−bath Hamiltonian of the form of eq 1 and the following choice of projection operator which gives rise to the GQME for the system reduced density matrix, $\hat{\sigma}(t)$:

$$\mathcal{P}(\hat{A}) = \hat{\rho}_n(0) \otimes \mathrm{Tr}_n\{\hat{A}\} \tag{5}$$

With this choice of $\mathcal{P}$, we have $\mathcal{Q}(\hat{\rho}_n(0)) = 0$. Plugging eq 5 into eq 4 and tracing over the nuclear (bath) Hilbert space leads to the GQME in eq 3. The memory kernel in eq 3 is given by

$$\mathcal{K}(\tau) = \frac{1}{\hbar^2}\mathrm{Tr}_n\{\mathcal{L}\mathrm{e}^{-\mathrm{i}\mathcal{Q}\mathcal{L}\tau/\hbar}\mathcal{Q}\mathcal{L}\hat{\rho}_n(0)\} \tag{6}$$

and can be obtained by solving the following Volterra equation:[27]

$$\mathcal{K}(\tau) = \mathrm{i}\dot{\mathcal{F}}(\tau) - \frac{1}{\hbar}\mathcal{F}(\tau)\langle\mathcal{L}\rangle_n^0 + \mathrm{i}\int_0^\tau \mathrm{d}\tau'\, \mathcal{F}(\tau-\tau')\mathcal{K}(\tau') \tag{7}$$

Here $\mathcal{F}(\tau)$ and $\dot{\mathcal{F}}(\tau)$ are the so-called projection-free inputs (PFIs), which are given by

https://doi.org/10.1021/acs.jctc.3c00316
J. Chem. Theory Comput. 2023, 19, 4851−4862

$$\mathcal{F}(\tau) = \frac{1}{\hbar}\mathrm{Tr}_\mathrm{n}\{\mathcal{L}e^{-i\mathcal{L}\tau/\hbar}\hat{\rho}_\mathrm{n}(0)\}$$
$$\dot{\mathcal{F}}(\tau) = -\frac{i}{\hbar^2}\mathrm{Tr}_\mathrm{n}\{\mathcal{L}e^{-i\mathcal{L}\tau/\hbar}\mathcal{L}\hat{\rho}_\mathrm{n}(0)\} \quad (8)$$

The memory kernels for the spin-boson model used in this paper were adopted from ref 78, where they were obtained from quantum-mechanically exact PFIs calculated *via* the tensor-train thermo-field dynamics (TT-TFD) method.

The quantum open system's *non-unitary* time evolution superoperator, or propagator, $\mathcal{G}(t)$, is defined by

$$\hat{\sigma}(t) = \mathcal{G}(t)\hat{\sigma}(0) \quad (9)$$

Substituting eq 9 into eq 3 and noting that the GQME should be satisfied for an arbitrary choice of $\hat{\sigma}(0)$, it is straightforward to show that $\mathcal{G}(t)$ satisfies the same GQME as $\hat{\sigma}(t)$:

$$\frac{d}{dt}\mathcal{G}(t) = -\frac{i}{\hbar}\langle\mathcal{L}\rangle_\mathrm{n}^0\mathcal{G}(t) - \int_0^t d\tau\, \mathcal{K}(\tau)\mathcal{G}(t-\tau) \quad (10)$$

Thus, given the projected Liouvillian and memory kernel ($\langle\mathcal{L}\rangle_\mathrm{n}^0$ and $\mathcal{K}(\tau)$, respectively), $\mathcal{G}(t)$ can be obtained by solving eq 10 numerically, which in this work was accomplished *via* a Runge−Kutta fourth-order (RK4) algorithm.[28] This superoperator, $\mathcal{G}(t)$, serves a role similar to that of the Kraus operators in the operator sum representation and can also be dilated to a unitary form which can be implemented on a quantum computer. Importantly, while the Kraus operators are only known in closed form for the Markovian Lindblad equation, the nonunitary propagator $\mathcal{G}(t)$ can always be obtained from the formally exact GQME (see eq 10).

2.2. A GQME-Based Quantum Algorithm for Simulating Open Quantum System Dynamics. In this subsection, we describe the next step in the workflow outlined in Figure 2, namely, using the Sz.-Nagy unitary dilation procedure[79] to convert the non-unitary quantum open system propagator $\mathcal{G}(t)$ (see eqs 9 and 10) into a unitary propagator in an extended Hilbert space. It should be noted that the Sz.-Nagy unitary dilation procedure is one out of several methods that can convert non-unitary operators into unitary operators (*e.g.*, block-encoding represents an alternative method[80,81]).

The Sz.-Nagy unitary dilation procedure starts out by calculating the operator norm of $\mathcal{G}(t)$ to determine whether it is a *contraction*. For $\mathcal{G}(t)$ to be a contraction, the operator norm of $\mathcal{G}(t)$ needs to be less than or equal to 1, *i.e.*, $\|\mathcal{G}(t)\|_\mathrm{O} = \sup\frac{\|\mathcal{G}(t)\boldsymbol{v}\|}{\|\boldsymbol{v}\|} \leq 1$. In the case where the original $\mathcal{G}(t)$ is *not* a contraction, we introduce a normalization factor $n_\mathrm{c} = \|\mathcal{G}(t)\|_\mathrm{O}$ in order to define a contraction form of $\mathcal{G}(t)$, namely, $\mathcal{G}'(t) = \mathcal{G}(t)/n_\mathrm{c}$.

In the next step, we apply a 1-dilation procedure to $\mathcal{G}'(t)$ to obtain a unitary propagator $\mathcal{U}_{\mathcal{G}'}(t)$ in an extended Hilbert space of double the dimension of the original system's Hilbert space:

$$\mathcal{U}_{\mathcal{G}'}(t) = \begin{pmatrix} \mathcal{G}'(t) & \mathcal{D}_{\mathcal{G}'^\dagger}(t) \\ \mathcal{D}_{\mathcal{G}'}(t) & -\mathcal{G}'^\dagger(t) \end{pmatrix} \quad (11)$$

In this equation, $\mathcal{D}_{\mathcal{G}'}(t) = \sqrt{I - \mathcal{G}'^\dagger(t)\mathcal{G}'(t)}$ and $\mathcal{D}_{\mathcal{G}'^\dagger} = \sqrt{I - \mathcal{G}'(t)\mathcal{G}'^\dagger(t)}$, where $\mathcal{D}_{\mathcal{G}'}(t)$ is the so-called defect superoperator of $\mathcal{G}'(t)$. The 1-dilation procedure generates a unitary superoperator $\mathcal{U}_{\mathcal{G}'}(t)$ that operates in the extended Hilbert space and replicates the effect of the contraction form of the original time evolution superoperator, $\mathcal{G}'(t)$, when the input and output vectors are both projected onto the original smaller Hilbert space.

In the original system's Hilbert space, the system reduced density operator $\hat{\sigma}(t)$ is represented by an $N_\mathrm{e} \times N_\mathrm{e}$ matrix:

$$\hat{\sigma}(t) \doteq \begin{pmatrix} \sigma_{11}(t) & \cdots & \sigma_{1N_\mathrm{e}}(t) \\ \vdots & \ddots & \vdots \\ \sigma_{N_\mathrm{e}1}(t) & \cdots & \sigma_{N_\mathrm{e}N_\mathrm{e}}(t) \end{pmatrix} \quad (12)$$

Alternatively, the same system reduced density operator can also be represented by an N_e^2-dimensional vector in Liouville space:

$$\hat{\sigma}(t) \doteq (\sigma_{11}(t), ..., \sigma_{1N_\mathrm{e}}(t), ..., \sigma_{N_\mathrm{e}1}(t), ..., \sigma_{N_\mathrm{e}N_\mathrm{e}}(t))^\mathrm{T} \quad (13)$$

Since the GQME formalism is given in terms of superoperators, it is convenient to work in Liouville space, which we will do from this point on. We also define the norm of the vector representing $\hat{\sigma}(t)$ in Liouville space as the Frobenius norm: $\|\sigma(t)\|_\mathrm{F} = \sqrt{\sum_{ij}|\sigma_{ij}|^2}$ and divide $\hat{\sigma}(t)$ by $\|\sigma(t)\|_\mathrm{F}$ to normalize $\hat{\sigma}(t)$.[68]

Given the dilated unitary operator $\mathcal{U}_{\mathcal{G}'}(t)$ and the initial quantum input state $\hat{\sigma}(0)$, operation with the non-unitary $\mathcal{G}'(t)$ on $\hat{\sigma}(0)$ has now been converted into a unitary transformation as follows:

$$\mathcal{G}'(t)\hat{\sigma}(0) \xrightarrow{\text{unitary dilation}} \mathcal{U}_{\mathcal{G}'}(t)(\hat{\sigma}(0)^\mathrm{T}, 0, ..., 0)^\mathrm{T} \quad (14)$$

The zeroes in the input vector on the R.H.S. are added to match the dimension of the input vector with that of $\mathcal{U}_{\mathcal{G}'}(t)$. The unitary process can then be simulated on a quantum circuit with unitary quantum gates. The electronic populations, $\{\sigma_{jj}(t) \equiv \langle j|\hat{\sigma}(t)|j\rangle | j = 1, ..., N_\mathrm{e}\}$, can be retrieved by taking the square root of the probability of measuring each basis state, $P_j(t) = |\sigma'_{jj}(t)|^2$, and multiplying by the n_c factor.

Finally, we perform a complexity analysis of the quantum algorithm. Given that $\mathcal{G}(t)$ in its most general form is represented by a matrix of N_e^4 nonzero elements, the defect superoperators $\mathcal{D}_{\mathcal{G}'}(t)$ and $\mathcal{D}_{\mathcal{G}'^\dagger}(t)$ as well as $-\mathcal{G}'^\dagger(t)$ as shown in eq 11 all have N_e^4 nonzero elements. Generally speaking, the number of two-level unitaries necessary to decompose a unitary gate is comparable to the number of nonzero elements in the lower-triangular part of the gate.[82,83] Therefore, the gate complexity to simulate this specific $\mathcal{U}_{\mathcal{G}'}(t)$ is $O(N_\mathrm{e}^4)$. If the two-level unitaries are further decomposed into 1-qubit and 2-qubit elementary gates commonly used to design conventional quantum circuits, they need to be transformed to the Gray code sequences and some multicontrol gate sequences, adding another factor of complexity logarithmic in N_e^2, and the total complexity becomes $O(N_\mathrm{e}^4 \log^2 N_\mathrm{e}^2)$.[82] This means that the maximum total complexity of a GQME-based simulation of the dynamics of an open quantum system is comparable to that of classical methods.[68] However, as demonstrated in previous simulations of certain dynamical models, our quantum algorithm can take advantage of the case when $\mathcal{G}(t)$ is a sparse

https://doi.org/10.1021/acs.jctc.3c00316
J. Chem. Theory Comput. 2023, 19, 4851−4862

Table 1. Spin-Boson Model and Simulation Parameters

	model parameters					numerical parameters		
model no.	ϵ	Γ	β	ξ	ω_c	ω_{max}	N_n	Δt
1	1.0Γ	1.0	$5.0\Gamma^{-1}$	0.1	1.0Γ	5Γ	60	$1.50083 \times 10^{-3}\Gamma^{-1}$
2	1.0Γ	1.0	$5.0\Gamma^{-1}$	0.1	2.0Γ	10Γ	60	$1.50083 \times 10^{-3}\Gamma^{-1}$
3	1.0Γ	1.0	$5.0\Gamma^{-1}$	0.4	2.0Γ	10Γ	60	$1.50083 \times 10^{-3}\Gamma^{-1}$
4	0.0Γ	1.0	$5.0\Gamma^{-1}$	0.2	2.5Γ	12Γ	60	$4.50249 \times 10^{-3}\Gamma^{-1}$

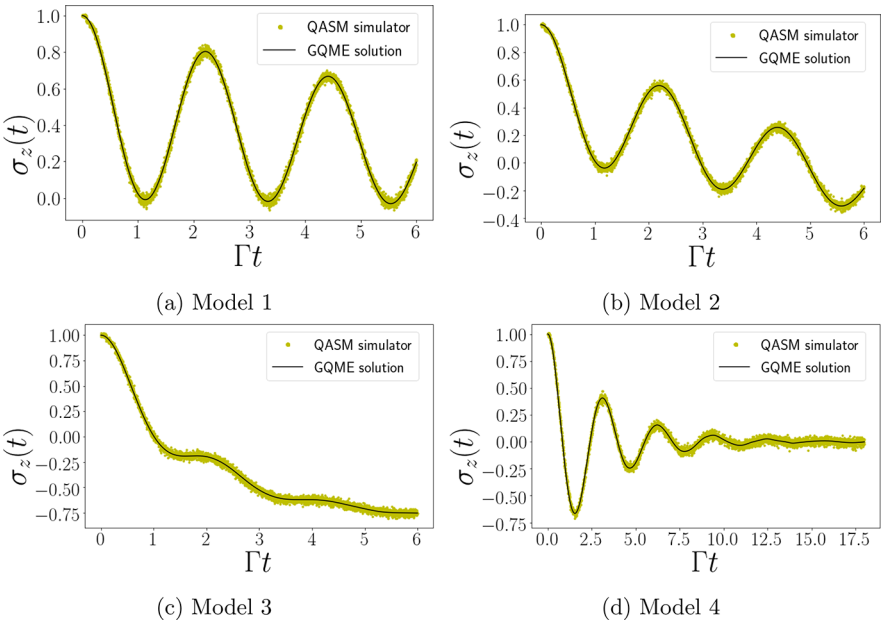

Figure 3. Spin-boson model simulated by the GQME-based quantum algorithm as implemented on the IBM QASM quantum simulator, showing the electronic population difference between the donor state and acceptor state, $\sigma_z(t) = \sigma_{DD}(t) - \sigma_{AA}(t)$, as a function of time for (a) model 1, (b) model 2, (c) model 3, and (d) model 4 as given in Table 1, with units scaled to the electronic coupling, Γ. Each panel shows the comparison between the GQME-based exact results (black curves) and the QASM-based results (yellow dots). The time step for both the exact and simulated results is $\Delta t = 1.50083 \times 10^{-3}\Gamma^{-1}$ for models 1−3 and $\Delta t = 4.50249 \times 10^{-3}\Gamma^{-1}$ for model 4. Each model is simulated for 4000 time steps. The number of projection measurements applied by the QASM simulator to obtain a single time step is 2000 shots.

matrix, and thus, the gate complexity scaling for $\mathcal{G}(t)$ can be reduced to $O(\log^2 N_e^2)$ instead of $O(N_e^4)$.[68,70]

3. RESULTS

3.1. A Demonstrative Application to the Spin-Boson Model. In this subsection, we test the applicability of the quantum algorithm outlined in the previous sections on the spin-boson benchmark model. This model and its derivatives have a wide range of applicability to chemical and physical systems, including electron, proton, energy, and charge transfer processes; polaron formation and dynamics in condensed-phase environments; vibrational relaxation; impurity relaxation in solids; spin−lattice relaxation; and qubit decoherence.[22,23,84,85] It should also be noted that quantum-mechanically exact memory kernels for this model are available.[78,86,87]

The spin-boson Hamiltonian has the form of eq 1 with $N_e = 2$ and $\{\hat{H}_j, \hat{V}_{jk}\}$ given by

$$\hat{H}_0 \equiv \hat{H}_D = \epsilon + \sum_{k=1}^{N_n} \frac{\hat{P}_k^2}{2} + \frac{1}{2}\omega_k^2 \hat{R}_k^2 - c_k \hat{R}_k$$

$$\hat{H}_1 \equiv \hat{H}_A = -\epsilon + \sum_{k=1}^{N_n} \frac{\hat{P}_k^2}{2} + \frac{1}{2}\omega_k^2 \hat{R}_k^2 + c_k \hat{R}_k$$

$$\hat{V}_{01} \equiv \hat{V}_{DA} = \hat{V}_{10} \equiv \hat{V}_{AD} = \Gamma \tag{15}$$

Here the two electronic states are designated as the donor and acceptor ($|D\rangle$ and $|A\rangle$, respectively), 2ϵ is the shift in equilibrium energy between the D and A states, and Γ is a positive constant describing the electronic coupling between the D and A states. Since Γ is a constant, this system is assumed to satisfy the Condon approximation.

The results shown below were obtained for the case where the nuclear modes' frequencies and coupling coefficients $\{\omega_k, c_k\}$ are sampled from an Ohmic spectral density with exponential cutoff:

$$J(\omega) = \frac{\pi}{2}\sum_{k=1}^{N_n} \frac{c_k^2}{\omega_k}\delta(\omega - \omega_k) \xrightarrow{N_n \to \infty} \frac{\pi\hbar}{2}\xi\omega e^{-\omega/\omega_c} \tag{16}$$

Here ξ is the Kondo parameter and ω_c is the cutoff frequency. The reader is referred to Appendix C of ref 27 for a description of the procedure used to obtain a discrete set of N_n nuclear mode

https://doi.org/10.1021/acs.jctc.3c00316
J. Chem. Theory Comput. 2023, 19, 4851−4862

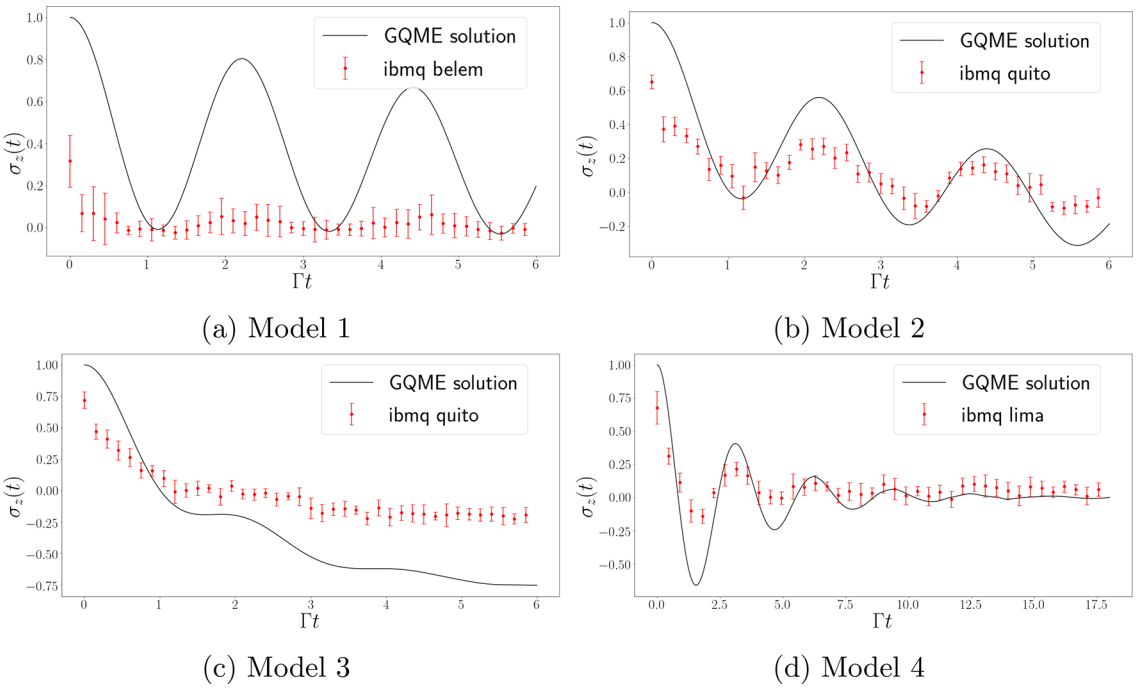

Figure 4. Spin-boson model simulated by the GQME quantum algorithm as implemented on the IBM quantum computers **ibmq belem**, **ibmq quito**, and **ibmq lima**, showing the electronic population difference between the donor state and acceptor state, $\sigma_z(t) = \sigma_{DD}(t) - \sigma_{AA}(t)$, as a function of time for (a) model 1, (b) model 2, (c) model 3, and (d) model 4 as given in Table 1, with units scaled to the electronic coupling, Γ. Each panel shows the comparison between the GQME-based exact results (black curves) and quantum-computer-based results (red dots with error bars). The time step for the real machine simulation is $\Delta t = 0.150083\Gamma^{-1}$ for models 1, 2, and 3 and $\Delta t = 0.450249\Gamma^{-1}$ for model 4. The experiments of both models take 40 evenly spaced time steps out of the 4000 time steps used in the QASM simulator runs, and the error bars represent the standard derivations of the 10 separate runs on **ibmq belem**, **ibmq quito**, and **ibmq lima** for models 1 to 4. The number of projection measurements applied by all the devices to obtain a single time step is 2000 shots.

frequencies $\{\omega_k\}$ and coupling coefficients $\{c_k\}$ from the spectral density in eq 16.

The initial state is assumed to be of the form of eq 2, with the initial electronic (system) reduced density operator given by

$$\hat{\sigma}(0) = |\mathrm{D}\rangle\langle\mathrm{D}| \tag{17}$$

and the initial nuclear (bath) reduced density operator given by

$$\hat{\rho}_n(0) = \frac{e^{-\beta(\hat{H}_D+\hat{H}_A)/2}}{\mathrm{Tr}_n\{e^{-\beta(\hat{H}_D+\hat{H}_A)/2}\}} \tag{18}$$

Calculations were carried out for four different sets of parameter values (see Table 1). Models 1 and 2 correspond to systems with an energy bias between the donor and acceptor states ($\epsilon \neq 0$) and differ in their cutoff frequencies, with model 2 having a higher cutoff frequency. Model 3 corresponds to a biased system with the same parameters as model 2 except for a larger Kondo parameter. Model 4 corresponds to a symmetric system with zero energy bias between the donor and acceptor states ($\epsilon = 0$). The results reported in this paper were obtained with a time step of $\Delta t = 1.50083 \times 10^{-3}\Gamma^{-1}$ for models 1−3 and a time step of $\Delta t = 4.50249 \times 10^{-3}\Gamma^{-1}$ for model 4.

Starting with the quantum-mechanically exact memory kernels (adopted from ref 78), the time evolution superoperator for the electronic reduced density matrix $\mathcal{G}(\tau)$ was generated for the four models given in Table 1 by solving the corresponding GQME (eq 10).

The GQME-based quantum algorithm for simulating the electronic dynamics within the spin-boson model was implemented on the IBM quantum platforms *via* the Qiskit package.[88] The quantum implementation involved the translation of $\mathcal{G}'(t)$ into $\mathcal{U}_{\mathcal{G}'}(t)$ at each time step, followed by the construction of a quantum circuit based on $\mathcal{U}_{\mathcal{G}'}(t)$ and the use of the quantum circuit to simulate the time evolution of the reduced electronic density matrix. To build the circuit, we dilated the 4×4 $\mathcal{G}'(t)$ into a unitary 8×8 $\mathcal{U}_{\mathcal{G}'}(t)$ by using a 1-dilation procedure (see eq 11]. The unitary $\mathcal{U}_{\mathcal{G}'}(t)$ was then transpiled into a 3-qubit quantum circuit composed of three elementary quantum gates: R_Z, $\sqrt{X}$, and CX. Examples of $\mathcal{U}_{\mathcal{G}'}(t)$ and details of the elementary quantum gates and circuits are given in the Supporting Information (SI). The initial electronic state is set to $(1, 0, 0, 0, 0, 0, 0, 0)^T$, where the last four zeroes are the extra dimensions from the dilation procedure. The QASM simulator and the real quantum devices initialize the input state $(1, 0, 0, 0, 0, 0, 0, 0)^T$ and apply the unitary operation $\mathcal{U}_{\mathcal{G}'}(t)$ to the input state followed by projection measurements to retrieve the probability distribution of all eight basis states. Each circuit runs 2000 shots, and the resulting probabilities $P_{000}(t)$ of measuring the state $|000\rangle$ and $P_{011}(t)$ of measuring $|011\rangle$ correspond to the diagonal elements of the modified density matrix, $|\sigma'_{00}(t)|^2$ and $|\sigma'_{11}(t)|^2$. The populations of the donor state, $\sigma_{00}(t)$, and acceptor state, $\sigma_{11}(t)$, are retrieved as follows:

$$\sigma_{00}(t) = \sqrt{P_{000}(t)} \times n_c \quad \text{and} \quad \sigma_{11}(t) = \sqrt{P_{011}(t)} \times n_c \tag{19}$$

In what follows, we report results in terms of the difference between the donor and acceptor populations, $\sigma_z(t) = \sigma_{00}(t) - \sigma_{11}(t)$.

https://doi.org/10.1021/acs.jctc.3c00316
J. Chem. Theory Comput. 2023, 19, 4851−4862

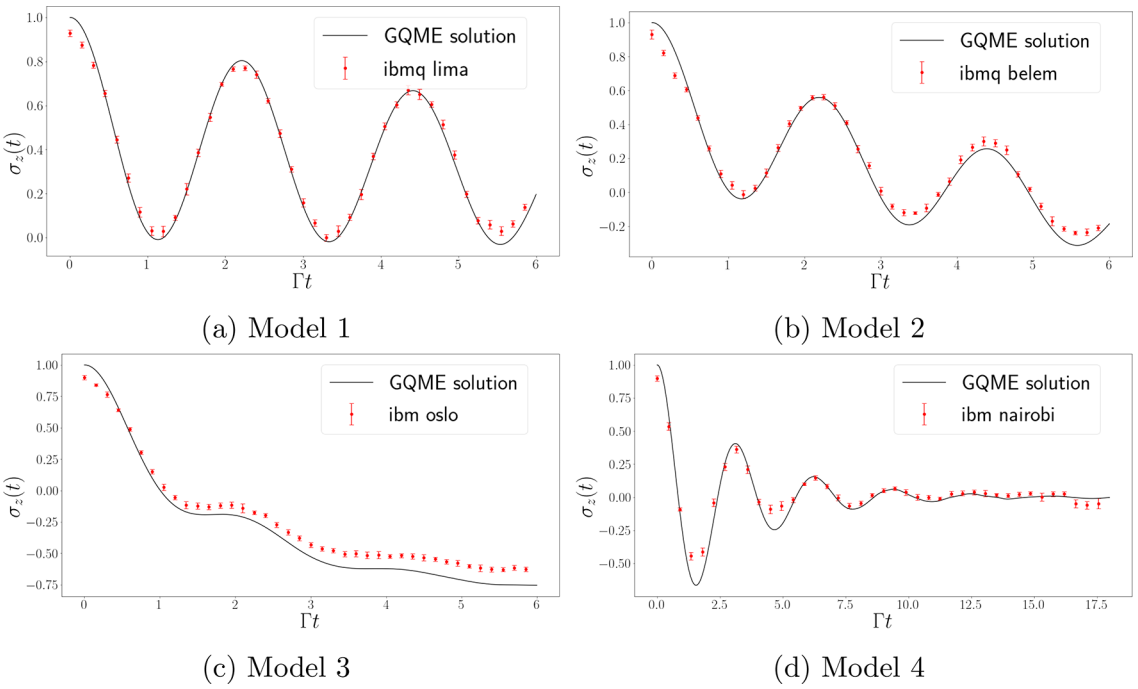

Figure 5. Comparison between the exact results for the spin-boson model and results obtained by performing the quantum algorithm based on eq 21 on the IBM Q quantum machines. The electronic population difference between the donor state and acceptor state, $\sigma_z(t) = \sigma_{DD}(t) - \sigma_{AA}(t)$, is plotted as a function of time for (a) model 1, (b) model 2, (c) model 3, and (d) model 4 as given in Table 1, with units scaled to the electronic coupling, Γ. Each panel shows the comparison between the exact results (black curves) and the population-only GQME-based quantum-computer-simulated results (red dots with error bars). The time step for the real machine simulation is $\Delta t = 0.150083\Gamma^{-1}$ for models 1, 2, and 3 and $\Delta t = 0.450249\Gamma^{-1}$ for model 4. The experiments of both models take 40 evenly spaced time steps out of the 4000 time steps used in the QASM simulator runs, and the error bars represent the standard derivations of the 10 separate runs on **ibmq lima**, **ibmq belem**, **ibm oslo**, and **ibm nairobi** for models 1−4, respectively. The number of projection measurements applied by all the devices to simulate a single time step is 2000 shots.

The comparison between the exact results obtained by solving the GQME on a classical computer and results obtained by performing the quantum algorithm on the QASM simulator is shown in Figure 3. The QASM simulator results are in excellent agreement with the exact results for all four models under consideration. The small-amplitude oscillations of the QASM-based results around the exact results can be traced back to the inherent uncertainty associated with projection measurements. These results validate the GQME-based quantum algorithm and demonstrate its ability to reproduce results obtained *via* the GQME-based classical algorithm.

To test the performance of the quantum algorithm on real quantum devices, we also performed the simulations on the quantum computers provided by IBM Quantum (IBM Q). The simulations were performed for models 1 to 4 on **ibmq quito**, **ibmq belem**, and **ibmq lima**. All devices are equipped with five qubits that have the same qubit connectivity and use IBM's **Falcon r4T** processor with the same architecture. In each simulation of a given model, three qubits were used, and 10 repeated experiments were performed. In a single experiment, 40 time steps are chosen at an equal spacing out of the 4000 time steps used in the QASM simulations, *i.e.*, the time step in each experiment is 100 times greater than the time step used in the QASM simulations as listed in Table 1. The average CX gate error and readout error are $(1.191 \times 10^{-2}, 5.194 \times 10^{-2})$ for **ibmq quito**, $(1.160 \times 10^{-2}, 2.590 \times 10^{-2})$ for **ibmq belem**, and $(1.032 \times 10^{-2}, 2.834 \times 10^{-2})$ for **ibmq lima** as of the time of the experiments. The quantum circuits are the same in both the QASM simulations and the real machine simulations. The transpiled quantum gate counts for each of the $\mathcal{U}_{\mathcal{G}'}(t)$ superoperators are 153 R_Z gates, 98$\sqrt{X}$ gates, and 41 CX gates. The transpiling process is done internally by the Qiskit package, and examples of the quantum circuits can be found in the SI.

The comparison between the GQME-generated exact results and real machine simulations is given in Figure 4. In the figure, the red dots are the averages of the 10 experiments, and the error bars represent the standard derivations of the 10 experiments. While the results obtained on the IBM Q quantum computers reproduce some of the trends exhibited by the exact results, the agreement is qualitative at best. The lack of quantitative agreement can be traced back to the rather extensive circuit depth, which makes the calculation susceptible to noise. In the next section, we propose a way to lower the circuit depth and enhance the accuracy of the calculation on the IBM Q quantum computers by using reduced-dimensionality GQMEs.

3.2. Reduced-Dimensionality GQME-Based Propagators. Since the quantum algorithm on the QASM simulator was able to accurately reproduce the exact results, as shown in Figure 3, we attribute the lack of quantitative agreement between the exact results and the results obtained *via* the IBM Q quantum computers, as seen in Figure 4, to noise within the real quantum devices. If so, reducing the circuit depth would improve the accuracy. In this subsection, we validate this hypothesis by reducing the dimensionality of the non-unitary propagator $\mathcal{G}(t)$, thereby lowering the circuit depth to levels that allow for an accurate calculation on the NISQ quantum computers.

To this end, we take inspiration from reduced-dimensionality GQMEs, which correspond to EoMs for subsets of the open quantum system's reduced density matrix elements rather than

https://doi.org/10.1021/acs.jctc.3c00316
J. Chem. Theory Comput. 2023, 19, 4851−4862

the full reduced density matrix.[30,78] For example, for the spin-boson model described in section 3.1, the memory kernel in the GQME for the full reduced density matrix, $\hat{\sigma}(t)$, is a 4×4 matrix, while the memory kernel in the GQME for only the two populations (the diagonal elements of the reduced density matrix, $\sigma_{00}(t)$ and $\sigma_{11}(t)$) is a 2×2 matrix.[30,78] Below we demonstrate how one can take advantage of this reduced dimensionality to lower the circuit depth and thereby improve the accuracy of the simulation on quantum machines.

For the spin-boson model under consideration in this paper, the electronic populations can be propagated using only the four corner elements of $\mathcal{G}(t)$, *i.e.*,

$$\begin{pmatrix} \sigma_{11}(t) \\ \sigma_{22}(t) \end{pmatrix} = \begin{pmatrix} \mathcal{G}_{11,11}(t) & \mathcal{G}_{11,22}(t) \\ \mathcal{G}_{22,11}(t) & \mathcal{G}_{22,22}(t) \end{pmatrix} \begin{pmatrix} \sigma_{11}(0) \\ \sigma_{22}(0) \end{pmatrix} \tag{20}$$

It should be noted that this equality only holds when the initial electionic state is of the form $\hat{\sigma}(0) = \sum_{j=1}^{N_e} \sigma_{jj}(0)|j\rangle\langle j|$, which is consistent with the initial state under consideration in this paper (see eq 17). It should also be noted that eq 20 is still exact, in the sense that the time evolution of $\sigma_{11}(t)$ and $\sigma_{00}(t)$ as described by the equation is exactly the same time evolution as described by eq 9. Thus, the only price one pays for the reduced dimensionality is the loss of the ability to simulate the dynamics of the off-diagonal matrix elements $\sigma_{10}(t)$ and $\sigma_{01}(t)$. However, given that the primary goal is often to simulate the dynamics of electronic energy/charge transfer, the populations of the corresponding electronic states is all that one needs. Finally, it is worth noting that our specific way of choosing the subset of the density operator does not indicate that there is no coupling between the elements. In fact, such coupling can be captured exactly by the memory kernel and the effective Liouvillian of any open quantum system with the GQME.

The 2×2 propagator in eq 20, which we will refer to as $\mathcal{G}^{\text{pop}}(t)$, can be dilated following a procedure similar to that used to dilate the 4×4 propagator for the full density matrix, $\mathcal{G}(t)$. More specifically, $\mathcal{G}^{\text{pop}}(t)$ can be divided by a normalization factor $n_c^{\text{pop}} = \|\mathcal{G}^{\text{pop}}(t)\|_{\text{O}}$ to obtain its contraction form $\mathcal{G}^{\text{pop}\prime}(t) = \mathcal{G}^{\text{pop}}(t)/n_c^{\text{pop}}$. Applying a 1-dilation procedure to $\mathcal{G}^{\text{pop}\prime}(t)$, similar to that in eq 11, then leads to the following unitary propagator:

$$\mathcal{U}_{\mathcal{G}^{\text{pop}\prime}}(t) = \begin{pmatrix} \mathcal{G}^{\text{pop}\prime}(t) & \mathcal{D}_{\mathcal{G}^{\text{pop}\prime\dagger}}(t) \\ \mathcal{D}_{\mathcal{G}^{\text{pop}\prime}}(t) & -\mathcal{G}^{\text{pop}\prime\dagger}(t) \end{pmatrix} \tag{21}$$

Notably, for the spin-boson model, while $\mathcal{U}_{\mathcal{G}'}(t)$ is an 8×8 time-dependent matrix, $\mathcal{U}_{\mathcal{G}^{\text{pop}\prime}}(t)$ is a 4×4 time-dependent matrix.

A comparison between the exact results and results obtained by performing the quantum algorithm based on eq 21 on IBM Q quantum machines is shown in Figure 5. The results shown were obtained for models 1−4 on **ibmq belem**, **ibmq lima**, **ibm oslo**, and **ibm nairobi**, respectively. Here, **ibm oslo** and **ibm nairobi** are each equipped with seven qubits of the same qubit connectivity, and both use IBM's **Falcon r5.11H** processor. The average *CX* gate error and readout error are $(1.038 \times 10^{-2}, 2.280 \times 10^{-2})$ for **ibm nairobi** and $(8.537 \times 10^{-3}, 2.310 \times 10^{-2})$ for **ibm oslo** as of the time of the experiments. The new simulations use the same time steps and experiment shots and follow the same procedures as used to obtain the results in Figure 4. The quantum circuits are retranspiled to implement the reduced-dimensionality GQME-based quantum algorithm where only two qubits are used. The transpiled quantum gate counts for each of the $\mathcal{U}_{\mathcal{G}^{\text{pop}\prime}}(t)$ superoperators are 17 R_Z gates, 12 $\sqrt{X}$ gates, and 2 *CX* gates. The transpiling processes are done internally by the Qiskit package.

The results in Figure 5 confirm that the lack of quantitative agreement seen in Figure 4 can be attributed to noise on the real quantum devices. More specifically, significantly more accurate results are obtained when the populations-only reduced-dimensionality GQME-based propagators are used, which can be traced back to their ability to give rise to shallower quantum circuits. Thus, reduced dimensionality makes it possible to accurately simulate the open quantum system dynamics on NISQ quantum computers.

4. CONCLUDING REMARKS

The GQME-based quantum algorithm proposed herein substantially expands the range of open quantum systems that can be simulated on a quantum computer. In this paper, we have demonstrated the applicability and versatility of the algorithm by using it to simulate the dynamics of electronic populations within the benchmark spin-boson model on the IBM QASM quantum simulator and IBM quantum computers.

The results obtained *via* the noise-free QASM simulator were found to be highly accurate, with the only errors inherently associated with the quantum projection measurements and giving rise to very slight deviations from the exact results. However, while the implementation of the algorithm on the NISQ IBM Q quantum computers was found to reproduce some of the trends exhibited by the exact results, the agreement was qualitative at best. This lack of quantitative agreement was traced back to the rather extensive circuit depth, which made the calculation susceptible to noise. This issue was confirmed and fixed by implementing a populations-only reduced-dimensionality version of the quantum algorithm, which significantly shortened the circuit depth and as a result gave rise to quantitatively accurate results.

We acknowledge the fact that demonstrating quantum advantage is currently challenging for the proposed quantum algorithm used to simulate open quantum dynamics. However, quantum dynamics simulations often become computationally intractable on a classical computer even when the propagator is known (or numerically determined). This is simply because the time-evolving state becomes highly entangled and therefore requires an exponentially large N memory space, where N is the number of possible states in Hilbert space (and an exponentially large computational effort). In contrast, a quantum computer can efficiently represent the time-evolving state with only $\log_2(N)$ qubits. In addition, further improvement to our quantum simulations can be achieved by reducing the circuit depth *via* optimizing the quantum circuit design. This can be achieved by optimizing the decomposition of unitary operations into elementary gate sequences.[89−92] One particularly interesting idea is to reduce the circuit depth by adding qubits.[93] To this end, it should be noted that we have only used three qubits out of the five currently available on the IBM quantum computers. Another way to improve accuracy is by active error correction using dynamical decoupling (DD) protocols, which employ pulses to suppress the system's coupling with the environment.[94−98] Recent implementations of DD on IBM machines was found to improve the fidelity of the overall perform-

https://doi.org/10.1021/acs.jctc.3c00316
J. Chem. Theory Comput. 2023, 19, 4851−4862

ance.[99−101] Yet another direction is to implement the circuit on high-dimensional qudit machines. Quantum computers based on three-dimensional circuit quantum electrodynamics (3D cQED) microwave cavities are particularly promising in this respect, as they feature unique quantum error correction schemes[102−104] and longer coherence times[105,106] than standard superconducting quantum computers. Bosonic quantum computing algorithms have also been recently shown to significantly reduce the number of quantum gates required for the calculation of the Franck−Condon factors[107] and dynamics of rhodopsin near conical intersections.[108] Lossless 3D cQED systems have not yet been employed to simulate open quantum system dynamics. An adaptation of the algorithm presented here to bosonic quantum computing could therefore provide another way to efficiently simulate open quantum system dynamics and demonstrate how qudit-based quantum architectures can reduce the computational cost and enhance the accuracy of quantum simulations.

■ ASSOCIATED CONTENT

Supporting Information

The Supporting Information is available free of charge at https://pubs.acs.org/doi/10.1021/acs.jctc.3c00316.

Examples of $\mathcal{U}_{G'}(t)$ and details of the elementary quantum gates and circuits (PDF)

■ AUTHOR INFORMATION

Corresponding Authors

Eitan Geva − *Department of Chemistry, University of Michigan, Ann Arbor, Michigan 48109, United States;* orcid.org/0000-0002-7935-4586; Email: eitan@umich.edu

Victor S. Batista − *Department of Chemistry and Yale Quantum Institute, Yale University, New Haven, Connecticut 06511, United States;* orcid.org/0000-0002-3262-1237; Email: victor.batista@yale.edu

Sabre Kais − *Department of Chemistry, Department of Physics, and Purdue Quantum Science and Engineering Institute, Purdue University, West Lafayette, Indiana 47907, United States;* orcid.org/0000-0003-0574-5346; Email: kais@purdue.edu

Authors

Yuchen Wang − *Department of Chemistry, Department of Physics, and Purdue Quantum Science and Engineering Institute, Purdue University, West Lafayette, Indiana 47907, United States;* orcid.org/0000-0002-6025-6329

Ellen Mulvihill − *Department of Chemistry and Yale Quantum Institute, Yale University, New Haven, Connecticut 06511, United States*

Zixuan Hu − *Department of Chemistry, Department of Physics, and Purdue Quantum Science and Engineering Institute, Purdue University, West Lafayette, Indiana 47907, United States;* orcid.org/0000-0002-0752-3811

Ningyi Lyu − *Department of Chemistry and Yale Quantum Institute, Yale University, New Haven, Connecticut 06511, United States;* orcid.org/0000-0001-9239-9925

Saurabh Shivpuje − *Department of Chemistry, Department of Physics, and Purdue Quantum Science and Engineering Institute, Purdue University, West Lafayette, Indiana 47907, United States*

Yudan Liu − *Department of Chemistry, University of Michigan, Ann Arbor, Michigan 48109, United States*

Micheline B. Soley − *Department of Chemistry and Yale Quantum Institute, Yale University, New Haven, Connecticut 06511, United States; Department of Chemistry and Department of Physics, University of Wisconsin-Madison, Madison, Wisconsin 53706, United States*

Complete contact information is available at: https://pubs.acs.org/10.1021/acs.jctc.3c00316

Notes

The authors declare no competing financial interest.

■ ACKNOWLEDGMENTS

We acknowledge the financial support of the National Science Foundation under Award 2124511, CCI Phase I: NSF Center for Quantum Dynamics on Modular Quantum Devices (CQD-MQD). We acknowledge the use of IBM Quantum services for this work. The views expressed are those of the authors and do not reflect the official policy or position of IBM or the IBM Quantum team.

■ REFERENCES

(1) Wangsness, R. K.; Bloch, F. The dynamical theory of nuclear induction. *Phys. Rev.* **1953**, *89*, 728.

(2) Redfield, A. G. On the theory of relaxation processes. *IBM J. Res. Dev.* **1957**, *1*, 19.

(3) Bloch, F. Generalized theory of relaxation. *Phys. Rev.* **1957**, *105*, 1206.

(4) Haake, F. Statistical treatment of open systems by generalized master equations. *Springer Tracts Mod. Phys.* **1973**, *66*, 98.

(5) Yoon, B.; Deutch, J. M.; Freed, J. H. A comparison of generalized cumulant and projection operator methods in spin-relaxation theory. *J. Chem. Phys.* **1975**, *62*, 4687−4696.

(6) Lindblad, G. On the generators of quantum dynamical semigroups. *Commun. Math. Phys.* **1976**, *48*, 119.

(7) Gorini, V.; Kossokowski, A.; Sudarshan, E. C. G. Completely positive dynamical semigroups of N-level systems. *J. Math. Phys.* **1976**, *17*, 821.

(8) Oppenheim, I.; Shuler, K. E.; Weiss, G. H. *Stochastic Processes in Chemical Physics: The Master Equation*; MIT Press: Cambridge MA, 1977.

(9) Alicki, R.; Lendi, K. *Quantum Dynamical Semigroups and Applications*; Springer: Berlin, 1987.

(10) Grabert, H. *Projection Operator Techniques in Nonequilibrium Statistical Mechanics*; Springer: Berlin, 1982.

(11) Kubo, R.; Toda, M.; Hashitsume, N. *Statistical Physics II - Nonequilibrium Statistical Mechanics*; Springer: Berlin, 1983.

(12) Laird, B. B.; Budimir, J.; Skinner, J. L. Quantum-mechanical derivation of the Bloch equations: Beyond the weak coupling limit. *J. Chem. Phys.* **1991**, *94*, 4391.

(13) Van Kampen, N. G. *Stochastic Processes in Physics and Chemistry*; Elsevier: Amsterdam, 1992.

(14) Pollard, W. T.; Felts, A. K.; Friesner, R. A. The Redfield equation in condensed-phase quantum dynamics. *Adv. Chem. Phys.* **2007**, *XCIII*, 77.

(15) Kohen, D.; Marston, C. C.; Tannor, D. J. Phase space approach to theories of quantum dissipation. *J. Chem. Phys.* **1997**, *107*, 5236−5253.

(16) Kosloff, R.; Ratner, M. A.; Davis, W. B. Dynamics and relaxation in interacting systems: Semigroup approach. *J. Chem. Phys.* **1997**, *106*, 7036.

(17) Cao, J. Phase space study of Bloch-Redfield theory. *J. Chem. Phys.* **1997**, *107*, 3204.

(18) Shi, Q.; Geva, E. Stimulated Raman Adiabatic Passage in The Presence of Dephasing. *J. Chem. Phys.* **2003**, *119*, 11773−11787.

(19) Baiz, C.; Kubarych, K.; Geva, E. Molecular theory and simulation of coherence transfer in metal carbonyls and its signature on

multidimensional infrared spectra. *J. Phys. Chem. B* **2011**, *115*, 5322−5339.
(20) Zwanzig, R. *Nonequilibrium Statistical Mechanics*; Oxford University Press: New York, 2001.
(21) May, V.; Kühn, O. *Charge and Energy Transfer Dynamics in Molecular Systems*; Wiley-VCH: Weinheim, Germany, 2000.
(22) Nitzan, A. *Chemical Dynamics in Condensed Phases*; Oxford University Press: New York, 2006.
(23) Breuer, H.-P.; Petruccione, F. *The Theory of Open Quantum Systems*; Oxford University Press: Oxford, U.K., 2002.
(24) Jang, S. J. *Dynamics of Molecular Excitons*; Elsevier: Amsterdam, 2021.
(25) Lai, Y.; Geva, E. On simulating the dynamics of electronic populations and coherences via quantum master equations based on treating off-diagonal electronic coupling terms as a small perturbation. *J. Chem. Phys.* **2021**, *155*, 204101−19.
(26) Chen, H.; Lidar, D. A. Hamiltonian open quantum system toolkit. *Commun. Phys.* **2022**, *5*, 112.
(27) Mulvihill, E.; Schubert, A.; Sun, X.; Dunietz, B. D.; Geva, E. A modified approach for simulating electronically nonadiabatic dynamics via the generalized quantum master equation. *J. Chem. Phys.* **2019**, *150*, 034101.
(28) Mulvihill, E.; Lenn, K. M.; Gao, X.; Schubert, A.; Dunietz, B. D.; Geva, E. Simulating energy transfer dynamics in the Fenna-Matthews-Olson complex via the modified generalized quantum master equation. *J. Chem. Phys.* **2021**, *154*, 204109.
(29) Mulvihill, E.; Geva, E. A Road Map to Various Pathways for Calculating the Memory Kernel of the Generalized Quantum Master Equation. *J. Phys. Chem. B* **2021**, *125*, 9834−9852.
(30) Mulvihill, E.; Geva, E. Simulating the dynamics of electronic observables via reduced-dimensionality generalized quantum master equations. *J. Chem. Phys.* **2022**, *156*, 044119.
(31) Xu, D.; Schulten, K. Coupling of protein motion to electron transfer in a photosynthetic reaction center: investigating the low temperature behavior in the framework of the spin−boson model. *Chem. Phys.* **1994**, *182*, 91−117.
(32) Ishizaki, A.; Fleming, G. R. Quantum Coherence in Photosynthetic Light Harvesting. *Annu. Rev. Condens. Matter Phys.* **2012**, *3*, 333−361.
(33) Liddell, P. A.; Kuciauskas, D.; Sumida, J. P.; Nash, B.; Nguyen, D.; Moore, A. L.; Moore, T. A.; Gust, D. Photoinduced charge separation and charge recombination to a triplet state in a carotene-porphyrin-fullerene triad. *J. Am. Chem. Soc.* **1997**, *119*, 1400−1405.
(34) Liddell, P. A.; Kodis, G.; Moore, A. L.; Moore, T. A.; Gust, D. Photo switching of photoinduced electron transfer in a dithienylethene-porphyrin-fullerene triad molecule. *J. Am. Chem. Soc.* **2002**, *124*, 7668−7669.
(35) Brédas, J.-L.; Beljonne, D.; Coropceanu, V.; Cornil, J. Charge-Transfer and Energy-Transfer Processes in π-Conjugated Oligomers and Polymers: A Molecular Picture. *Chem. Rev.* **2004**, *104*, 4971−5004.
(36) Rizzi, A. C.; van Gastel, M.; Liddell, P. A.; Palacios, R. E.; Moore, G. F.; Kodis, G.; Moore, A. L.; Moore, T. A.; Gust, D.; Braslavsky, S. E. Entropic changes control the charge separation process in triads mimicking photosynthetic charge separation. *J. Phys. Chem. A* **2008**, *112*, 4215−4223.
(37) Tian, H.; Yu, Z.; Hagfeldt, A.; Kloo, L.; Sun, L. Organic Redox Couples and Organic Counter Electrode for Efficient Organic Dye-Sensitized Solar Cells. *J. Am. Chem. Soc.* **2011**, *133*, 9413−9422.
(38) Mishra, A.; Fischer, M. K. R.; Bäuerle, P. Metal-Free Organic Dyes for Dye-Sensitized Solar Cells: From Structure: Property Relationships to Design Rules. *Angew. Chem., Int. Ed.* **2009**, *48*, 2474−2499.
(39) Feldt, S. M.; Gibson, E. A.; Gabrielsson, E.; Sun, L.; Boschloo, G.; Hagfeldt, A. Design of Organic Dyes and Cobalt Polypyridine Redox Mediators for High-Efficiency Dye-Sensitized Solar Cells. *J. Am. Chem. Soc.* **2010**, *132*, 16714−16724.
(40) Zhao, Y.; Liang, W. Charge transfer in organic molecules for solar cells: Theoretical perspective. *Chem. Soc. Rev.* **2012**, *41*, 1075−1087.
(41) Lee, M. H.; Dunietz, B. D.; Geva, E. Calculation From First Principles of Intramolecular Golden-Rule Rate Constants for Photo-Induced Electron Transfer in Molecular Donor-Acceptor Systems. *J. Phys. Chem. C* **2013**, *117*, 23391−23401.
(42) Lee, M. H.; Dunietz, B. D.; Geva, E. Donor-to-Donor vs. Donor-to-Acceptor Interfacial Charge Transfer States in the Phthalocyanine-Fullerene Organic Photovoltaic System. *J. Phys. Chem. Lett.* **2014**, *5*, 3810−3816.
(43) Hu, Z.; Engel, G. S.; Alharbi, F. H.; Kais, S. Dark states and delocalization: Competing effects of quantum coherence on the efficiency of light harvesting systems. *J. Chem. Phys.* **2018**, *148*, 064304.
(44) Hu, Z.; Engel, G. S.; Kais, S. Double-excitation manifold's effect on exciton transfer dynamics and the efficiency of coherent light harvesting. *Phys. Chem. Chem. Phys.* **2018**, *20*, 30032−30040.
(45) Daley, A. J. Quantum trajectories and open many-body quantum systems. *Adv. Phys.* **2014**, *63*, 77−149.
(46) Wiseman, H. M.; Milburn, G. J. *Quantum Measurement and Control*; Cambridge University Press: Cambridge, U.K., 2009.
(47) Brian, D.; Sun, X. Generalized quantum master equation: A tutorial review and recent advances. *Chin. J. Chem. Phys.* **2021**, *34*, 497−524.
(48) Dan, X.; Xu, M.; Yan, Y.; Shi, Q. Generalized master equation for charge transport in a molecular junction: Exact memory kernels and their high order expansion. *J. Chem. Phys.* **2022**, *156*, 134114.
(49) Kais, S. Introduction to Quantum Information and Computation for Chemistry. In *Quantum Information and Computation for Chemistry*; Kais, S., Ed.; Advances in Chemical Physics, Vol. *154*; John Wiley & Sons: Hoboken, NJ, 2014; Chapter 1, pp 1−38.
(50) Peruzzo, A.; McClean, J.; Shadbolt, P.; Yung, M.-H.; Zhou, X.-Q.; Love, P. J.; Aspuru-Guzik, A.; O'Brien, J. L. A variational eigenvalue solver on a photonic quantum processor. *Nat. Commun.* **2014**, *5*, 4213.
(51) O'Malley, P. J. J.; Babbush, R.; Kivlichan, I. D.; Romero, J.; McClean, J. R.; Barends, R.; Kelly, J.; Roushan, P.; Tranter, A.; Ding, N.; Campbell, B.; Chen, Y.; Chen, Z.; Chiaro, B.; Dunsworth, A.; Fowler, A. G.; Jeffrey, E.; Lucero, E.; Megrant, A.; Mutus, J. Y.; Neeley, M.; Neill, C.; Quintana, C.; Sank, D.; Vainsencher, A.; Wenner, J.; White, T. C.; Coveney, P. V.; Love, P. J.; Neven, H.; Aspuru-Guzik, A.; Martinis, J. M. Scalable quantum simulation of molecular energies. *Phys. Rev. X* **2016**, *6*, 031007.
(52) Xia, R.; Bian, T.; Kais, S. Electronic structure calculations and the Ising Hamiltonian. *J. Phys. Chem. B* **2018**, *122*, 3384−3395.
(53) Xia, R.; Kais, S. Quantum machine learning for electronic structure calculations. *Nat. Commun.* **2018**, *9*, 4195.
(54) Wiebe, N.; Berry, D. W.; Høyer, P.; Sanders, B. C. Simulating quantum dynamics on a quantum computer. *J. Phys. A Math. Theor.* **2011**, *44*, 445308.
(55) Ollitrault, P. J.; Miessen, A.; Tavernelli, I. Molecular quantum dynamics: A quantum computing perspective. *Acc. Chem. Res.* **2021**, *54*, 4229−4238.
(56) Yao, Y.-X.; Gomes, N.; Zhang, F.; Wang, C.-Z.; Ho, K.-M.; Iadecola, T.; Orth, P. P. Adaptive variational quantum dynamics simulations. *PRX Quantum* **2021**, *2*, 030307.
(57) Tagliacozzo, L. Optimal simulation of quantum dynamics. *Nat. Phys.* **2022**, *18*, 970−971.
(58) Lloyd, S.; Viola, L. Engineering quantum dynamics. *Phys. Rev. A* **2001**, *65*, 010101.
(59) Wang, H.; Ashhab, S.; Nori, F. Quantum algorithm for simulating the dynamics of an open quantum system. *Phys. Rev. A* **2011**, *83*, 062317.
(60) Wang, D.-S.; Berry, D. W.; De Oliveira, M. C.; Sanders, B. C. Solovay-kitaev decomposition strategy for single-qubit channels. *Phys. Rev. Lett.* **2013**, *111*, 130504.
(61) Wei, S.-J.; Ruan, D.; Long, G.-L. Duality quantum algorithm efficiently simulates open quantum systems. *Sci. Rep.* **2016**, *6*, 30727.
(62) Kliesch, M.; Barthel, T.; Gogolin, C.; Kastoryano, M.; Eisert, J. Dissipative quantum church-turing theorem. *Phys. Rev. Lett.* **2011**, *107*, 120501.

https://doi.org/10.1021/acs.jctc.3c00316
J. Chem. Theory Comput. 2023, 19, 4851−4862

(63) Sweke, R.; Sinayskiy, I.; Bernard, D.; Petruccione, F. Universal simulation of Markovian open quantum systems. *Phys. Rev. A* **2015**, *91*, 062308.
(64) Schlimgen, A. W.; Head-Marsden, K.; Sager, L. M.; Narang, P.; Mazziotti, D. A. Quantum simulation of open quantum systems using a unitary decomposition of operators. *Phys. Rev. Lett.* **2021**, *127*, 270503.
(65) Zhang, Y.; Hu, Z.; Wang, Y.; Kais, S. Quantum Simulation of the Radical Pair Dynamics of the Avian Compass. *J. Phys. Chem. Lett.* **2023**, *14*, 832−837.
(66) Guimarães, J. D.; Lim, J.; Vasilevskiy, M. I.; Huelga, S. F.; Plenio, M. B. Noise-assisted digital quantum simulation of open systems. *arXiv (Quantum Physics)*, March 15, 2023, 2302.14592, ver. 2. https://arxiv.org/abs/2302.14592 (accessed 2023-03-19).
(67) Rossini, M.; Maile, D.; Ankerhold, J.; Donvil, B. I. Single Qubit Error Mitigation by Simulating Non-Markovian Dynamics. *arXiv (Quantum Physics)*, March 6, 2023, 2303.03268, ver. 1. https://arxiv.org/abs/2303.03268 (accessed 2023-03-19).
(68) Hu, Z.; Xia, R.; Kais, S. A quantum algorithm for evolving open quantum dynamics on quantum computing devices. *Sci. Rep.* **2020**, *10*, 3301.
(69) Head-Marsden, K.; Krastanov, S.; Mazziotti, D. A.; Narang, P. Capturing non-Markovian dynamics on near-term quantum computers. *Phys. Rev. Res.* **2021**, *3*, 013182.
(70) Hu, Z.; Head-Marsden, K.; Mazziotti, D. A.; Narang, P.; Kais, S. A general quantum algorithm for open quantum dynamics demonstrated with the Fenna-Matthews-Olson complex. *Quantum* **2022**, *6*, 726.
(71) Nakajima, S. On the quantum theory of transport phenomena. *Prog. Theor. Phys.* **1958**, *20*, 948−959.
(72) Zwanzig, R. Ensemble method in the theory of irreversibility. *J. Chem. Phys.* **1960**, *33*, 1338−1341.
(73) Pfalzgraff, W.; Montoya-Castillo, A.; Kelly, A.; Markland, T. Efficient construction of generalized master equation memory kernels for multi-state systems from nonadiabatic quantum-classical dynamics. *J. Chem. Phys.* **2019**, *150*, 244109−16.
(74) Fetherolf, J. H.; Berkelbach, T. C. Linear and nonlinear spectroscopy from quantum master equations. *J. Chem. Phys.* **2017**, *147*, 244109.
(75) Fay, T. P.; Lindoy, L. P.; Manolopoulos, D. E. Electron spin relaxation in radical pairs: Beyond the Redfield approximation. *J. Chem. Phys.* **2019**, *151*, 154117.
(76) Schile, A. J.; Limmer, D. T. Simulating conical intersection dynamics in the condensed phase with hybrid quantum master equations. *J. Chem. Phys.* **2019**, *151*, 014106.
(77) Rivas, Á.; Huelga, S. F. *Open Quantum Systems: An Introduction*; Springer: Berlin, 2012.
(78) Lyu, N.; Mulvihill, E.; Soley, M. B.; Geva, E.; Batista, V. S. Tensor-Train Thermo-Field Memory Kernels for Generalized Quantum Master Equations. *J. Chem. Theory Comput.* **2023**, *19*, 1111−1129.
(79) Levy, E.; Shalit, O. M. Dilation theory in finite dimensions: the possible, the impossible and the unknown. *Rocky Mountain J. Math.* **2014**, *44*, 203−221.
(80) Gilyén, A.; Su, Y.; Low, G. H.; Wiebe, N. Quantum singular value transformation and beyond: exponential improvements for quantum matrix arithmetics. In *Proceedings of the 51st Annual ACM SIGACT Symposium on Theory of Computing*; Association for Computing Machinery: New York, 2019; pp 193−204.
(81) Camps, D.; Lin, L.; Van Beeumen, R.; Yang, C. Explicit Quantum Circuits for Block Encodings of Certain Sparse Matrice. *arXiv (Quantum Physics)*, February 3, 2023, 2203.10236, ver. 3. https://arxiv.org/abs/2203.10236 (accessed 2023-03-19).
(82) Nielsen, M. A.; Chuang, I. L. *Quantum Computation and Quantum Information: 10th Anniversary Edition*; Cambridge University Press: Cambridge, U.K., 2011.
(83) Reck, M.; Zeilinger, A.; Bernstein, H. J.; Bertani, P. Experimental realization of any discrete unitary operator. *Phys. Rev. Lett.* **1994**, *73*, 58−61.
(84) Leggett, A. J.; Chakravarty, S.; Dorsey, A. T.; Fisher, M. P. A.; Garg, A.; Zwerger, W. Dynamics of the dissipative two-state system. *Rev. Mod. Phys.* **1987**, *59*, 1−85.
(85) Weiss, U. *Quantum Dissipative Systems*, 4th ed.; World Scientific: Singapore, 2012.
(86) Shi, Q.; Geva, E. A new approach to calculating the memory kernel of the generalized quantum master equation for an arbitrary system−bath coupling. *J. Chem. Phys.* **2003**, *119*, 12063−12076.
(87) Chatterjee, S.; Makri, N. Real-Time Path Integral Methods, Quantum Master Equations, and Classical vs Quantum Memory. *J. Phys. Chem. B* **2019**, *123*, 10470−10482.
(88) Aleksandrowicz, G.; Alexander, T.; Barkoutsos, P.; Bello, L.; Ben-Haim, Y.; Bucher, D.; Cabrera-Hernández, F. J.; Carballo-Franquis, J.; Chen, A.; Chen, C.-F.; Chow, J. M.; Córcoles-Gonzales, A. D.; Cross, A. J.; Cross, A.; Cruz-Benito, J.; Culver, C.; González, S. D. L. P.; Torre, E. D. L.; Ding, D.; Dumitrescu, E.; Duran, I.; Eendebak, P.; Everitt, M.; Sertage, I. F.; Frisch, A.; Fuhrer, A.; Gambetta, J.; Gago, B. G.; Gomez-Mosquera, J.; Greenberg, D.; Hamamura, I.; Havlicek, V.; Hellmers, J.; Herok, Ł.; Horii, H.; Hu, S.; Imamichi, T.; Itoko, T.; Javadi-Abhari, A.; Kanazawa, N.; Karazeev, A.; Krsulich, K.; Liu, P.; Luh, Y.; Maeng, Y.; Marques, M.; Martín-Fernández, F. J.; McClure, D. T.; McKay, D.; Meesala, S.; Mezzacapo, A.; Moll, N.; Rodríguez, D. M.; Nannicini, G.; Nation, P.; Ollitrault, P.; O'Riordan, L. J.; Paik, H.; Pérez, J.; Phan, A.; Pistoia, M.; Prutyanov, V.; Reuter, M.; Rice, J.; Davila, A. R.; Rudy, R. H. P.; Ryu, M.; Sathaye, N.; Schnabel, C.; Schoute, E.; Setia, K.; Shi, Y.; Silva, A.; Siraichi, Y.; Sivarajah, S.; Smolin, J. A.; Soeken, M.; Takahashi, H.; Tavernelli, I.; Taylor, C.; Taylour, P.; Trabing, K.; Treinish, M.; Turner, W.; Vogt-Lee, D.; Vuillot, C.; Wildstrom, J. A.; Wilson, J.; Winston, E.; Wood, C.; Wood, S.; Wörner, S.; Akhalwaya, I. Y.; Zoufal, C. *Qiskit: An Open-source Framework for Quantum Computing*, 2019; DOI: 10.5281/zenodo.2562111.
(89) Vartiainen, J. J.; Möttönen, M.; Salomaa, M. M. Efficient decomposition of quantum gates. *Phys. Rev. Lett.* **2004**, *92*, 177902.
(90) Gyongyosi, L. Quantum state optimization and computational pathway evaluation for gate-model quantum computers. *Sci. Rep.* **2020**, *10*, 4543.
(91) Lacroix, N.; Hellings, C.; Andersen, C. K.; Di Paolo, A.; Remm, A.; Lazar, S.; Krinner, S.; Norris, G. J.; Gabureac, M.; Heinsoo, J.; Blais, A.; Eichler, C.; Wallraff, A. Improving the performance of deep quantum optimization algorithms with continuous gate sets. *PRX Quantum* **2020**, *1*, 020304.
(92) Iten, R.; Moyard, R.; Metger, T.; Sutter, D.; Woerner, S. Exact and practical pattern matching for quantum circuit optimization. *ACM Trans. Quantum Comput* **2022**, *3*, 1−41.
(93) Abdessaied, N.; Wille, R.; Soeken, M.; Drechsler, R. Reducing the depth of quantum circuits using additional circuit lines. In *International Conference on Reversible Computation*; Springer: Berlin, 2013; pp 221−233.
(94) Viola, L.; Lloyd, S. Dynamical suppression of decoherence in two-state quantum systems. *Phys. Rev. A* **1998**, *58*, 2733.
(95) Uhrig, G. S. Keeping a quantum bit alive by optimized π-pulse sequences. *Phys. Rev. Lett.* **2007**, *98*, 100504.
(96) Khodjasteh, K.; Lidar, D. A. Fault-tolerant quantum dynamical decoupling. *Phys. Rev. Lett.* **2005**, *95*, 180501.
(97) Khodjasteh, K.; Lidar, D. A. Performance of deterministic dynamical decoupling schemes: Concatenated and periodic pulse sequences. *Phys. Rev. A* **2007**, *75*, 062310.
(98) West, J. R.; Fong, B. H.; Lidar, D. A. Near-optimal dynamical decoupling of a qubit. *Phys. Rev. Lett.* **2010**, *104*, 130501.
(99) Pokharel, B.; Anand, N.; Fortman, B.; Lidar, D. A. Demonstration of fidelity improvement using dynamical decoupling with superconducting qubits. *Phys. Rev. Lett.* **2018**, *121*, 220502.
(100) Das, P.; Tannu, S.; Dangwal, S.; Qureshi, M. Adapt: Mitigating idling errors in qubits via adaptive dynamical decoupling. In *MICRO-54:54th Annual IEEE/ACM International Symposium on Microarchitecture*; Association for Computing Machinery: New York, 2021; pp 950−962.
(101) Jurcevic, P.; Javadi-Abhari, A.; Bishop, L. S.; Lauer, I.; Bogorin, D. F.; Brink, M.; Capelluto, L.; Günlük, O.; Itoko, T.; Kanazawa, N.;

Kandala, A.; Keefe, G. A.; Krsulich, K.; Landers, W.; Lewandowski, E. P.; McClure, D. T.; Nannicini, G.; Narasgond, A.; Nayfeh, H. M.; Pritchett, E.; Rothwell, M. B.; Srinivasan, S.; Sundaresan, N.; Wang, C.; Wei, K. X.; Wood, C. J.; Yau, J.-B.; Zhang, E. J.; Dial, O. E.; Chow, J. M.; Gambetta, J. M. Demonstration of quantum volume 64 on a superconducting quantum computing system. *Quantum Sci. Technol.* **2021**, *6*, 025020.

(102) Ofek, N.; Petrenko, A.; Heeres, R.; Reinhold, P.; Leghtas, Z.; Vlastakis, B.; Liu, Y.; Frunzio, L.; Girvin, S.; Jiang, L.; Mirrahimi, M.; Devoret, M. H.; Schoelkopf, R. J. Extending the lifetime of a quantum bit with error correction in superconducting circuits. *Nature* **2016**, *536*, 441−445.

(103) Hu, L.; Ma, Y.; Cai, W.; Mu, X.; Xu, Y.; Wang, W.; Wu, Y.; Wang, H.; Song, Y.; Zou, C.-L.; Girvin, S. M.; Duan, L.-M.; Sun, L. Quantum error correction and universal gate set operation on a binomial bosonic logical qubit. *Nat. Phys.* **2019**, *15*, 503−508.

(104) Campagne-Ibarcq, P.; Eickbusch, A.; Touzard, S.; Zalys-Geller, E.; Frattini, N. E.; Sivak, V. V.; Reinhold, P.; Puri, S.; Shankar, S.; Schoelkopf, R. J.; Frunzio, L.; Mirrahimi, M.; Devoret, M. H. Quantum error correction of a qubit encoded in grid states of an oscillator. *Nature* **2020**, *584*, 368−372.

(105) Paik, H.; Schuster, D. I.; Bishop, L. S.; Kirchmair, G.; Catelani, G.; Sears, A. P.; Johnson, B. R.; Reagor, M. J.; Frunzio, L.; Glazman, L. I.; Girvin, S. M.; Devoret, M. H.; Schoelkopf, R. J. Observation of high coherence in Josephson junction qubits measured in a three-dimensional circuit QED architecture. *Phys. Rev. Lett.* **2011**, *107*, 240501.

(106) Reagor, M.; Pfaff, W.; Axline, C.; Heeres, R. W.; Ofek, N.; Sliwa, K.; Holland, E.; Wang, C.; Blumoff, J.; Chou, K.; Hatridge, M. J.; Frunzio, L.; Devoret, M. H.; Jiang, L.; Schoelkopf, R. J. Quantum memory with millisecond coherence in circuit QED. *Phys. Rev. B* **2016**, *94*, 014506.

(107) Wang, C. S.; Curtis, J. C.; Lester, B. J.; Zhang, Y.; Gao, Y. Y.; Freeze, J.; Batista, V. S.; Vaccaro, P. H.; Chuang, I. L.; Frunzio, L.; Jiang, L.; Girvin, S. M.; Schoelkopf, R. J. Efficient multiphoton sampling of molecular vibronic spectra on a superconducting bosonic processor. *Phys. Rev. X* **2020**, *10*, 021060.

(108) Wang, C. S.; Frattini, N. E.; Chapman, B. J.; Puri, S.; Girvin, S. M.; Devoret, M. H.; Schoelkopf, R. J. Observation of wave-packet branching through an engineered conical intersection. *Phys. Rev. X* **2023**, *13*, No. 011008.

https://doi.org/10.1021/acs.jctc.3c00316
J. Chem. Theory Comput. 2023, 19, 4851−4862